

PAPER • OPEN ACCESS

Direct fabrication and characterization of vertically stacked Graphene/h-BN/Graphene tunnel junctions

To cite this article: Ali Alzahrani *et al* 2021 *Nano Ex.* 2 040010

View the [article online](#) for updates and enhancements.

You may also like

- [Growth and characterization of uniformly distributed triangular single-crystalline hexagonal boron nitride grains on liquid copper surface](#)
Ziqiang Hao, Xuechao Liu, Xinfeng Zhu et al.
- [Growth of h-BN/graphene heterostructure using proximity catalysis](#)
Hui Yang, Bojun Wang, Xiaobin Niu et al.
- [Orientation-dependent mechanical response of graphene/BN hybrid nanostructures](#)
Lokanath Patra, Govind Mallick, Geeta Sachdeva et al.



PAPER

Direct fabrication and characterization of vertically stacked Graphene/h-BN/Graphene tunnel junctions

OPEN ACCESS

RECEIVED

20 August 2021

REVISED

24 September 2021

ACCEPTED FOR PUBLICATION

11 October 2021

PUBLISHED

22 December 2021

Ali Alzahrani^{1,2,*}, Adel Alruqi³, Bhupendra Karki¹, Milinda Kalutara Koralalage¹, Jacek Jasinski⁴ and Gamini Sumanasekera^{1,4}¹ Department of Physics & Astronomy, University of Louisville, Louisville, KY, 40292, United States of America² Department of Physics, Al-Qunfudah University college, Umm Al-Qura University, Makkah, 21955, Saudi Arabia³ Department of Physics, King Abdulaziz University, Jeddah, 21589, Saudi Arabia⁴ Conn Center for Renewable Energy Research, University of Louisville, Louisville, KY, 40292, United States of America

* Author to whom any correspondence should be addressed.

E-mail: ali.alzahrani@louisville.edu**Keywords:** graphene, h-BN, chemical vapor deposition, resonant tunneling, heterostructures, 2D-materials, negative differential resistanceSupplementary material for this article is available [online](#)

Original content from this work may be used under the terms of the [Creative Commons Attribution 4.0 licence](#).

Any further distribution of this work must maintain attribution to the author(s) and the title of the work, journal citation and DOI.

**Abstract**

We have used a lithography free technique for the direct fabrication of vertically stacked two-dimensional (2D) material-based tunnel junctions and characterized by Raman, AFM, XPS. We fabricated Graphene/h-BN/Graphene devices by direct deposition of graphene (bottom layer), h-BN (insulating barrier) and graphene (top layer) sequentially using a plasma enhanced chemical vapor deposition on Si/SiO₂ substrates. The thickness of the h-BN insulating layer was varied by tuning the plasma power and the deposition time. Samples were characterized by Raman, AFM, and XPS. The I-V data follows the barrier thickness dependent quantum tunneling behavior for equally doped graphene layers. The resonant tunneling behavior was observed at room temperature for oppositely doped graphene layers where hydrazine and ammonia were used for n-doping of one of the graphene layers. The resonance with negative differential conductance occurs when the band structures of the two electrodes are aligned. The doping effect of the resonant peak is observed for varying doping levels. The results are explained according to the Bardeen tunneling model.

1. Introduction

The tunneling transport phenomenon in quantum devices offers picosecond switching speeds and hence the possibility of designing very high-speed devices. Two-dimensional electron gas (2DEG) systems have played a vital role in the development of superior electronic devices [1]. However, one lesser-known device that utilized 2DEGs is a tunnel junction consisting of two such gases [2, 3], realizing 2D–2D tunneling. Previous studies of 2D–2D tunneling were conducted on coupled electron gas systems in two closely placed quantum wells in AlGaAs/GaAs heterostructures [3, 4]. In the case of unequal doping of the 2DEGs, it has been shown experimentally that, at a voltage bias corresponding to aligned band structures of the 2D systems, a sharp peak in the tunnel current occurs [1, 5–8]. This peak is referred as a resonant peak in the tunneling. It was claimed in the prior work that the width of this resonant peak was temperature independent (except possibly from inelastic effects) [6, 9–11].

Presence of negative differential resistance (NDR) is characteristic of the current–voltage relationship of a resonant tunneling device [12], enabling many unique applications [13]. The existence of devices with NDR has been reported since the late 1950's in devices that contained degenerately doped p-n junctions with thin oxide barriers (tunnel diodes) and double barrier heterojunction devices [14] where quantum tunneling effects are utilized. The NDR in the I-V characteristics of these devices has been used in many applications [15] involving microwave/millimeter wave oscillators, high speed logic devices and switches.

With the advent of the new 2D electronic material systems, it has opened a new route for 2D–2D tunneling in such extended systems [16]. Two-dimensional(2D) materials such as graphene, hexagonal-boron nitride (h-BN), transition

metal dichalcogenides (TMDCs) and phosphorene etc have gained a vast interest due to their excellent performance in novel electronic, optoelectronic and photovoltaic applications [17–22]. Graphene and h-BN have been unsuitable for electronics applications which require tunable band gap materials since graphene is metallic while h-BN being wide band gap semiconductor [23]. Strong reactivity of phosphorene, with oxygen and water and requires to be sandwiched between layers of other materials if it is to last longer than a few hours [24]. TMDCs are much slower conductors of electrons than graphene or phosphorene, even though they are semiconducting and stable. In order to evade such limitations, researchers have attempted a combination of metallic (graphene etc), insulating (h-BN etc) and semiconducting (MoS₂ etc) [25], 2D materials to facilitate functional heterostructure devices. Features of this approach include; adding some functionality into such 2D structures [26–28], combining into nanocomposites to optimize many inherent properties such as optical absorption etc [29, 30] and, stacking them vertically layer-by-layer or arrange laterally by seamlessly stitched in-plane heterojunctions [31–33].

Heterostructures play a vital role in semiconductor industry. The newly developed monolayer 2D materials offer a platform that allows creation of heterostructures with a variety of novel properties [34]. Many structural, physical, and chemical properties have been explored on Van der Waals heterostructures created by monolayers of multiple 2D materials with vertically stacked layered heterojunctions [35–39]. Since these heterostructures utilize the Van der Waals interlayer interaction, lattice matching is no longer a significant factor. The interface is atomically sharp, and the junction can be as thin as two atomic layers to reach the ultimate limits. Such stacks are very different from the traditional 3D semiconductor heterostructures, as each layer acts simultaneously as the bulk material and the surface and thereby reducing the amount of charge displacement within each layer. In addition, these structures are flexible and stable with compatible fabrication thin-film technologies.

In recent years, there have been various studies on graphene-2D materials heterostructures demonstrating novel charge transport properties across the interface [38, 40, 41]. Such graphene-TMDs structures have been introduced for various device applications and, also been of particular interest in the spectroscopy community [38, 42–44]. For example, many groups demonstrated the vertical tunneling transistors with high on-off ratios and large current densities that used TMDs thin layers as tunneling barriers and graphene as one or both electrodes [34, 35, 38, 40, 45].

An ideal 2D material for next generation of functional devices should meet the following important criteria. They must be (i) one-atom thick (for fastest conduction of electrons), (ii) be highly stable (even at high temperatures), (iii) possess a small and tunable band gap and, (iv) scalable in both synthesis and processing with the ability to integrate with existing technology etc.

Lithography methods in various forms are widely used in many research fields for making functional devices, including tunnel junctions. In the traditional top-down lithography technology, high-cost equipment including pre-designed masks and collimated light sources are used, which also include complex and time-consuming production steps. Electron beam lithography has capability to write nanoscale patterns without using any physical mask [46], but again the expensive equipment and low patterning speed associated with it suppress its extensive applications [47]. Further, 2D materials having single or few atomic layers, are particularly sensitive to surface contaminants, including resist residues left behind by lithographical processes, which in turn modify the electrochemical potential and act as extra scattering sites. Though annealing techniques have been demonstrated to improve device mobility [48, 49], they are not well controlled and do not always yield consistent results.

However, the employment of a vertical geometry enables overcome of both (i) the lithographical limitations inherent with in-planar geometry and (ii) poor scalability still sustaining large current modulations. Thus, there has been significantly increased interest on improving bottom-up techniques of lithography-free patterning in recent years. To achieve regular nanoscale patterns without using any mask, techniques like laser interference and nanosphere lithography have been developed as alternative routes [50]. Lithography-free fabrication techniques have been reported especially for simple geometries yielding simple, inexpensive [51], and free of resist processing with increased device throughput. Most importantly, lithography free techniques can be used by anybody who doesn't have access to clean room facility.

Chemical vapor deposition (CVD) has been found to be the best technique to synthesize uniform and large-scale graphene on metal substrates such as Copper and Nickel foils [52–58]. However, high processing temperatures (1000 °C–1600 °C) of thermal CVD growth of graphene [59–61] is costly and limits its direct applications in certain devices. The graphene films grown on metals need to be separated from the metal substrates and then transferred to insulating substrates (e.g., dielectrics, insulators) for further electronic processing [62]. Currently, the most common approach to transfer graphene is the use of polymethyl-methacrylate (PMMA) or polydimethylsiloxane (PDMS) [63–66]. The appearance of cracks or tears, and contamination of PMMA into graphene are inevitable during such complicated transfer procedures. In this regard, plasma-enhanced CVD (PECVD) has been commonly employed to synthesize transfer-free graphene and graphene nano-walls on different substrates including both metals and insulators at lower synthesis temperature [67–74].

Here, we experimentally investigate the possibility of using graphene/h-BN/graphene in direct quantum tunnel junctions [75] and resonant tunneling devices. With the recent advancements of synthesis of graphene and h-BN on

any arbitrary substrate using PECVD and fabrication of vertically stacked electronic devices using a simple lithography free technique allows us to address this question easily and rapidly since h-BN has great potential to be used as the tunneling barrier layer in functional heterostructure devices. The combination of graphene and h-BN opens up the exciting possibility of creating a new class of atomically thin multilayered heterostructures. In particular, this work focuses on the situations when the two graphene sheets have unequal doping, e.g., one is n-type (electron doped) in a single tunnel junction device and the other is p-type (hole doped). In this study, graphene and h-BN were directly deposited by radio frequency-plasma enhanced chemical vapor deposition (RF-PECVD) [76]. In the case of graphene, methane (CH_4) gas was used whilst ammonia borane was used for h-BN synthesis [77].

2. Experimental

Graphene was directly deposited on Si/SiO₂ substrate using RF-PECVD technique developed in our laboratory [78]. A home-made split ring radiofrequency (13.56 MHz, Max. power 600 W) system was used for plasma generation. Proper cleaning of the substrate is a required to avoid any kind of contamination prior to synthesizing the graphene layer as a thin film on the entire Si/SiO₂ substrate. Therefore, all the substrates were sonicated in acetone for 10 min and dried in a flow of nitrogen before placing them inside the quartz reactor. Then the reactor was evacuated to a pressure lower than ~5 mTorr and gradually heated to 650 °C in a flowing gas mixture: Ar/H₂ (40 vol% argon, 60 vol% H₂) at a flow rate of ~20 standard cubic centimeter per minute (sccm). The pressure was maintained at ~200 mTorr during this temperature ramp. Hydrogen plasma was ignited at the power of 50 W for 20 min after the heating step. Pure CH₄ (99.8%) at a flow rate of ~3 sccm was introduced into the growth chamber immediately after switching off the Ar/H₂ and plasma power of ~80 W was maintained for 30 ~ 120 min. The samples were then cooled down to room temperature at a rate 25 °C min⁻¹. [79]

Next, we prepared the sample for the deposition of h-BN using PECVD with ammonia borane (with 97% purity) as the source material [80]. The substrate with previously deposited graphene layer was covered with a circular shadow mask was placed inside the reactor at a desired position. Then, a ceramic boat containing borane ammonia borane was located in between the plasma reactor and the furnace. A heat belt was wrapped over the quartz tube covering the ceramic boat to sublime borane ammonia. Then the reactor was evacuated until the pressure lower than ~5 mTorr and gradually heated to 750 °C with the gas mixture: Ar/H₂ (40 vol % argon, 60 vol % H₂) at a flow rate of ~50 sccm. The ceramic boat was heated gradually from room temperature up to 180 °C and left for 45 min. and the plasma was maintained at 100 W [81]. The samples were then cooled down to room temperature at a rate 25 °C min⁻¹. Finally, the third graphene layer was deposited as before using another mask with a smaller opening[34].

As prepared graphene shows p-type behaviour. To be used in resonant tunneling devices, it was n-doped by exposing to hydrazine at room temperature. The graphene sample was placed inside a reactor which was connected to a vial containing hydrazine. The reactor was pumped and hydrazine was admitted to a pressure of 10 Torr in sequence. We also synthesized n-type graphene directly by PECVD using anhydrous ammonia with CH₄. Same procedure as in the synthesis of p-type graphene was followed except that ammonia gas was introduced along with CH₄ as a dopant for 10 min. Figure 1 shows the aforementioned sequential processes of fabricating graphene/h-BN/graphene-based device. The top row in figure 1 represents the schematic diagrams while the bottom row show the optical images of the sample after each step. (a) bare Si/SiO₂ substrate (b) Si/SiO₂ substrate completely coated with graphene (c) h-BN patch defined on the bottom graphene layer using a circular mask (6 mm diameter) (d) final graphene top layer deposited on the h-BN patch using a circular mask (3 mm diameter)

3. Characterization

Graphene and h-BN films were characterized by Raman spectroscopy with a spectral resolution better than 1 cm⁻¹. A Renishaw inVia spectrometer with a grating of 1800 lines mm⁻¹, a charge-coupled device (CCD) detector was used with 632 nm laser excitation. Figure 2 shows the Raman spectrum of graphene and h-BN. The Raman peaks of graphene appearing at 1346 cm⁻¹, 1596 cm⁻¹, 1628 cm⁻¹, and 2677 cm⁻¹ are characteristic of D, G, D', and 2D bands of graphene. The D (1346 cm⁻¹) band is known as the disorder band associated with the defects of graphene. G (1596 cm⁻¹) is a primary in-plane vibrational mode involving the sp² hybridized carbon atoms that comprises the graphene sheet. The D'-band (around 1628 cm⁻¹) is associated with edges and structural disorder in graphene films [82]. 2D or G' (2677 cm⁻¹), is the second-order overtone of the D band corresponding the result of a two-phonon lattice vibrational process. The full width at half maximum (FWHM) of G band and 2D band are 32 cm⁻¹ and 64 cm⁻¹ respectively. The intensity ratio between G band and 2D band, $\frac{I_G}{I_{2D}}$ is 0.82. The PECVD technique allows the growth of graphene on both conductive and insulated substrates with almost the same quality. The Raman spectrum of h-BN consisting of a peak at ~1367 cm⁻¹ with the FWHM of 13 cm⁻¹ which is assigned to the high-frequency vibrational mode (E_{2g})[34].

X-ray photoemission spectroscopy was also used to analyze the synthesized 2D films. XPS analysis was performed using a VG Scientific MultiLab 3000 ultra-high vacuum surface analysis system with a dual-anode (Mg/Al) x-ray source,

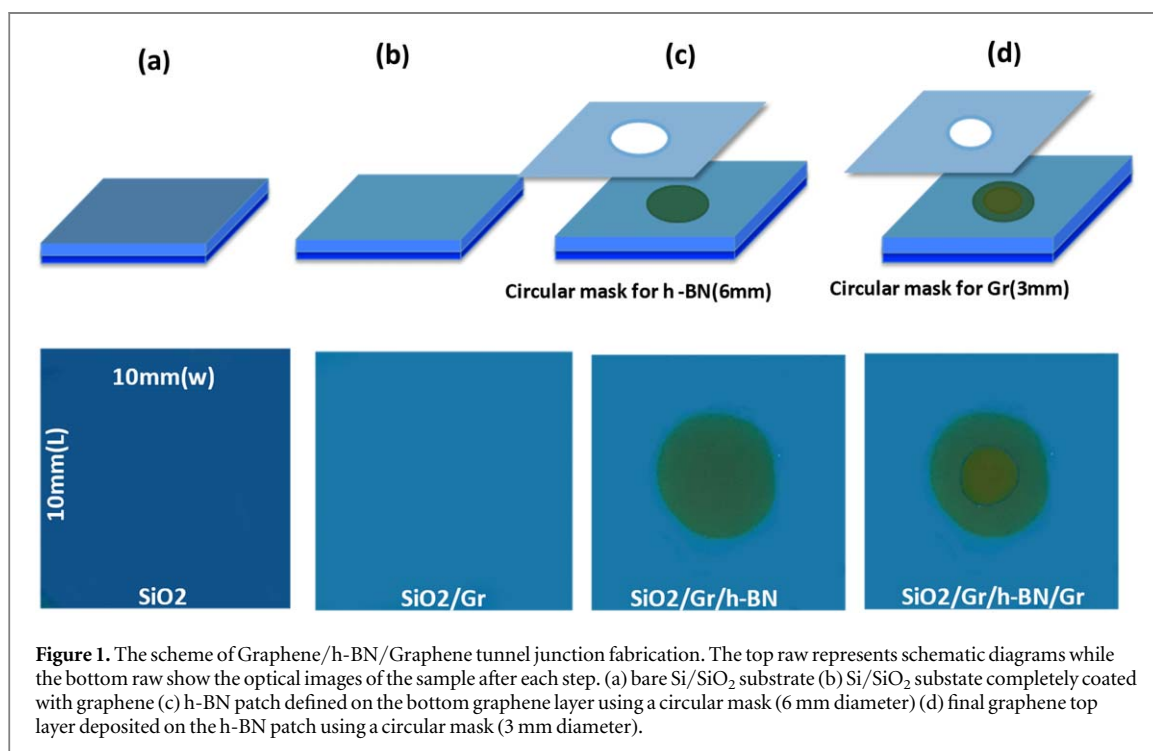


Figure 1. The scheme of Graphene/h-BN/Graphene tunnel junction fabrication. The top row represents schematic diagrams while the bottom row show the optical images of the sample after each step. (a) bare Si/SiO₂ substrate (b) Si/SiO₂ substrate completely coated with graphene (c) h-BN patch defined on the bottom graphene layer using a circular mask (6 mm diameter) (d) final graphene top layer deposited on the h-BN patch using a circular mask (3 mm diameter).

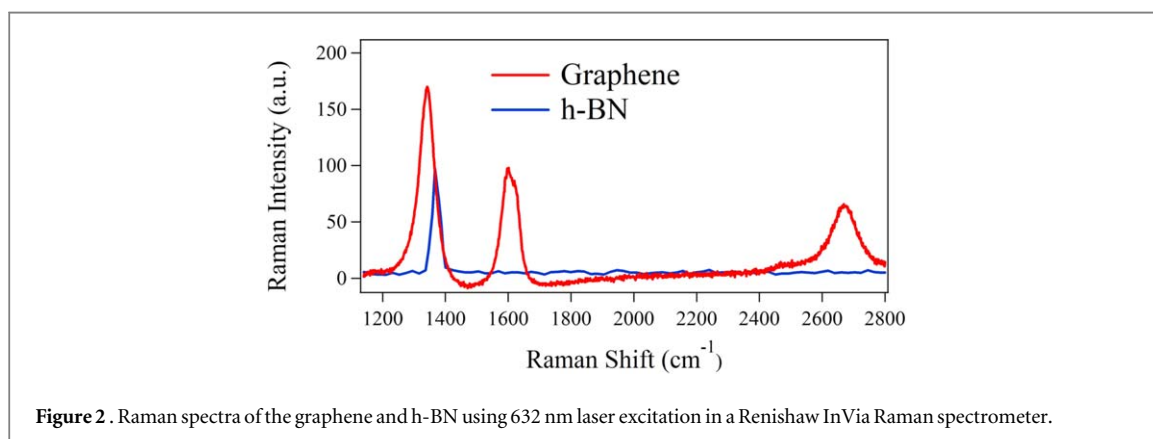


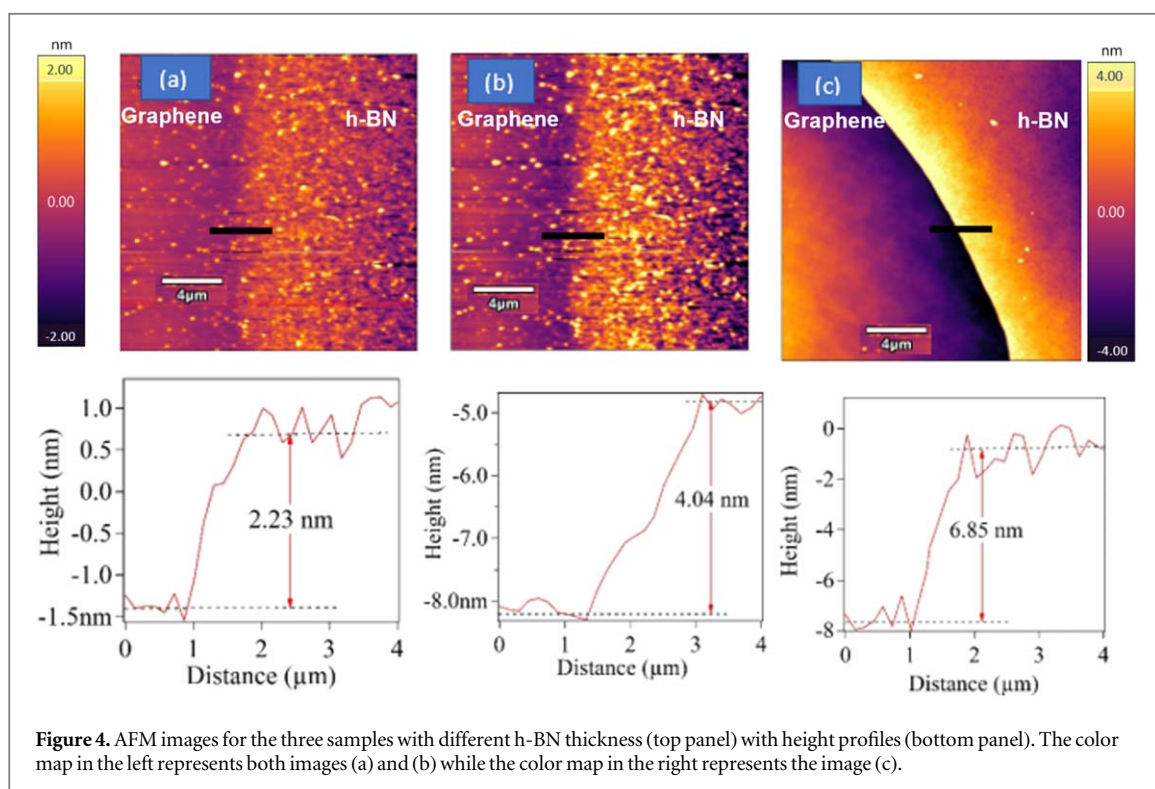
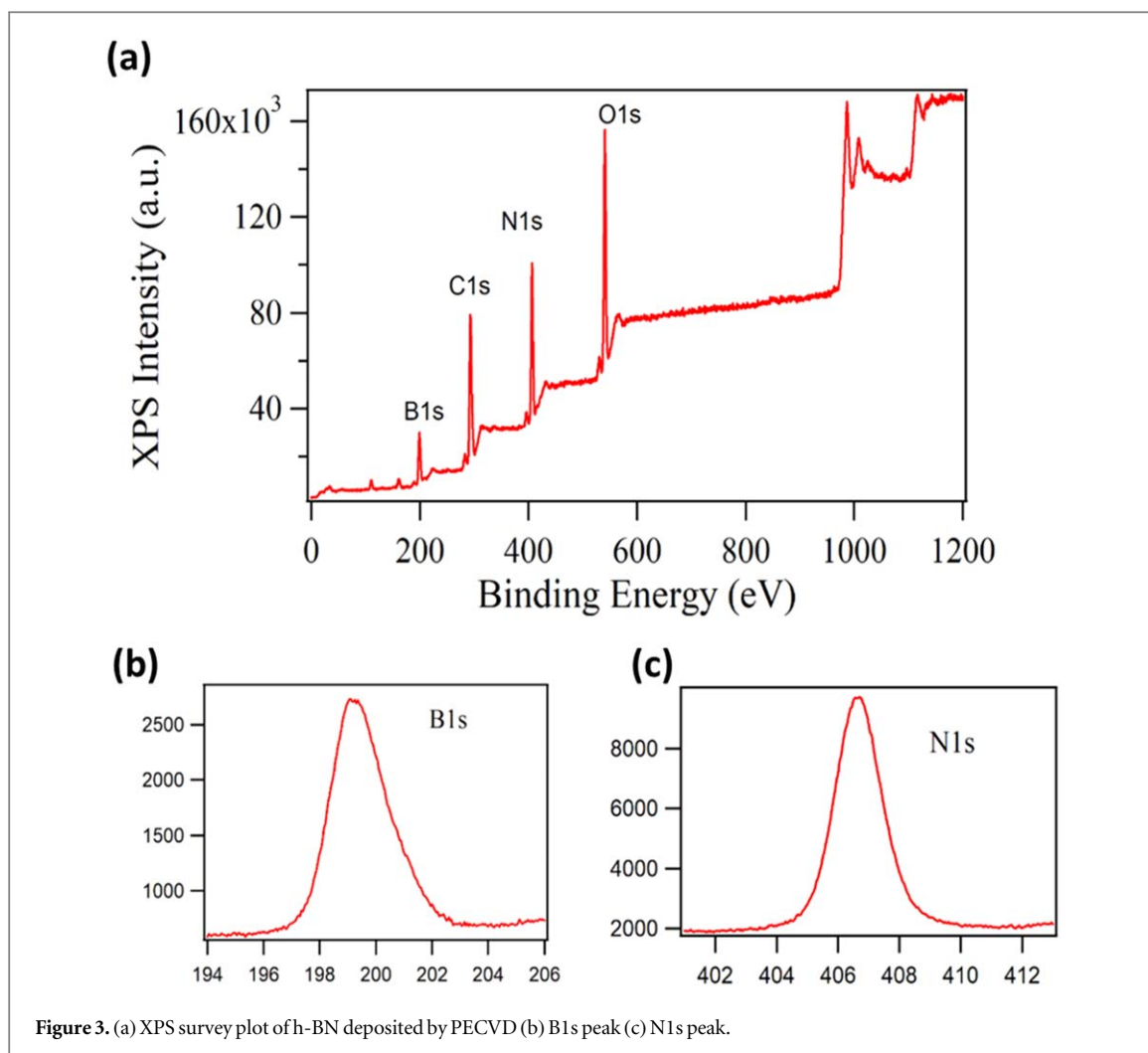
Figure 2. Raman spectra of the graphene and h-BN using 632 nm laser excitation in a Renishaw InVia Raman spectrometer.

a CLAM4 hemispherical electron energy analyzer, and at a base pressure of 10^{-9} Torr was used for x-ray photoelectron spectroscopy (XPS) measurements. The measurements were conducted using a non-monochromatized Al K α x-ray radiation ($h\nu \approx 1486.6$ eV) at a base pressure of 10^{-9} Torr. The C-C (sp^2) peak of adventitious carbon at 284.5 eV was used for the binding energy (BE) calibration. Figure 3 shows the x-ray photo-emission spectroscopy (XPS) results of h-BN grown by PECVD. The survey spectrum shown in figure 3(a) clearly shows the presence of boron and nitrogen with the appearance of XPS peaks corresponding to B1s and N1s core electrons [34]. As expected, an additional peak corresponding to O1s core electrons is also present in the survey spectrum. The unexpected peak characteristic of C1s core electrons is presumably due to the carbon contamination resulting from previous synthesis of graphene in the same reactor. Figures 3 (b) and (c) show the high-resolution individual peaks, B1s and N1s at the binding energies (BE) 198.6 eV and 406.8 eV, respectively. These BEs are consistent with the reported XPS characteristic values for h-BN. Stoichiometry evaluation based on B1s and N1s peak areas gives B/N ratio of 1.08, suggesting equal composition of B and N elements in h-BN.

4. Results

4.1. Direct quantum tunneling

Figure 4 shows AFM images (of the surface) and height profile of each sample taken by an Asylum Research MFP-3D-Bio atomic force microscope. The AFM topography images were obtained in tapping mode in air with the aid of Si tips with a typical tip radius of 25 nm, tip length of ~ 240 μm , spring constant range $1.8 - 12.5$ N m^{-1} ,



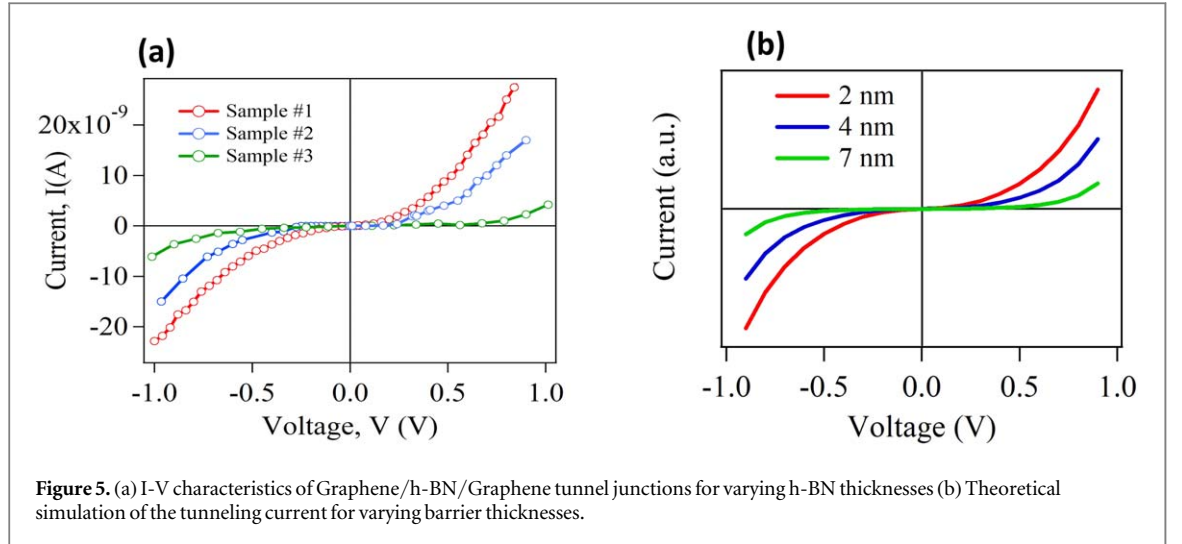


Figure 5. (a) I-V characteristics of Graphene/h-BN/Graphene tunnel junctions for varying h-BN thicknesses (b) Theoretical simulation of the tunneling current for varying barrier thicknesses.

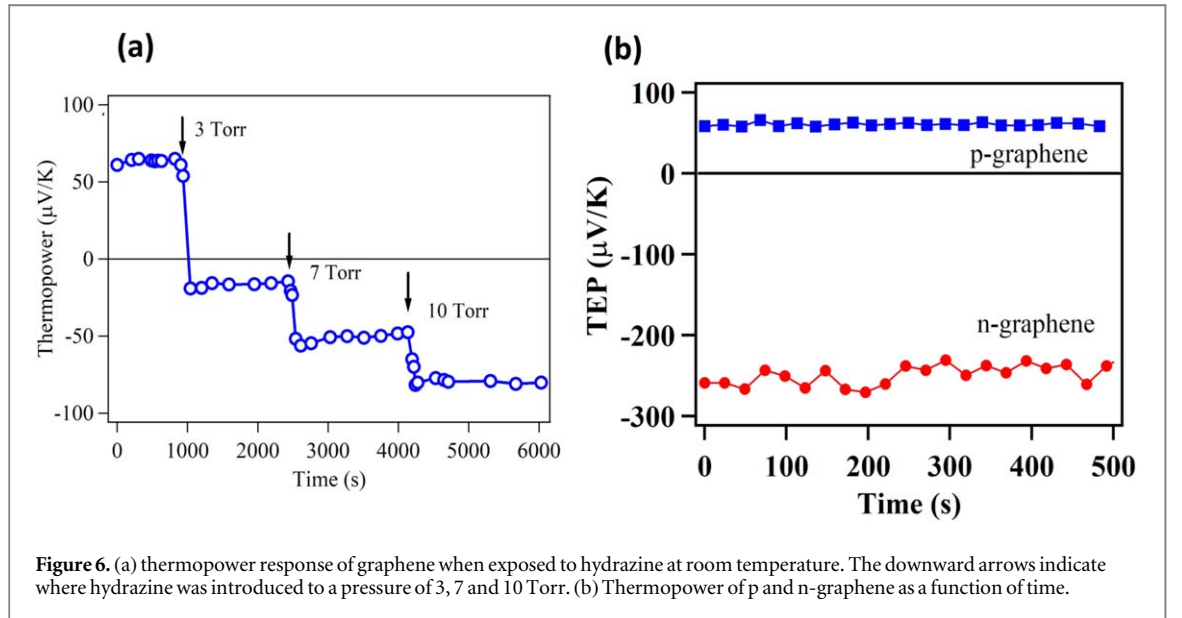


Figure 6. (a) thermopower response of graphene when exposed to hydrazine at room temperature. The downward arrows indicate where hydrazine was introduced to a pressure of 3, 7 and 10 Torr. (b) Thermopower of p and n-graphene as a function of time.

and frequency range 58–97 kHz. The average thicknesses of samples were found to be 2.23, 4.04, and 6.85 nm respectively [83]

Figure 5 shows the tunneling I-V characteristic curves of three Graphene/h-BN/Graphene based single tunnel junctions with varying h-BN thicknesses (tunnel barrier widths). All three curves show exponential dependence of the current (I) with the bias voltage (V) at higher voltages. We also calculated the slope of the linear range of each curve about $V = 0$ to evaluate the zero-bias conductivity (ZBC). The ZBC of the samples were found to be $1.760 \text{ G}\Omega^{-1}$, $0.356 \text{ G}\Omega^{-1}$ and $0.025 \text{ G}\Omega^{-1}$ as the h-BN barrier width increases from the thinnest to the thickest, revealing the exponential dependence of the ZBC with the barrier width [34].

We will simulate the tunneling current using the following formalism [6]. The tunneling current, I can be expressed as,

$$I = g_s g_v e \sum_{\alpha, \beta} \left\{ \frac{1}{\tau_{\alpha\beta}} f_T(E_\alpha) [1 - f_B(E_\beta)] - \frac{1}{\tau_{\beta\alpha}} f_R(E_\beta) [1 - f_T(E_\alpha)] \right\} \quad (1)$$

where, α and β represent the top (T) and bottom (B) electrodes with energies, E_α and E_β respectively, $g_s = 2$ is the spin degeneracy and g_v is the valley degeneracy, $\tau_{\alpha\beta}$ and $\tau_{\beta\alpha}$ are the tunneling rates for electrons tunneling from top \rightarrow bottom and bottom \rightarrow top respectively and f_T and f_B are Fermi occupation factor for the top and bottom electrodes given by,

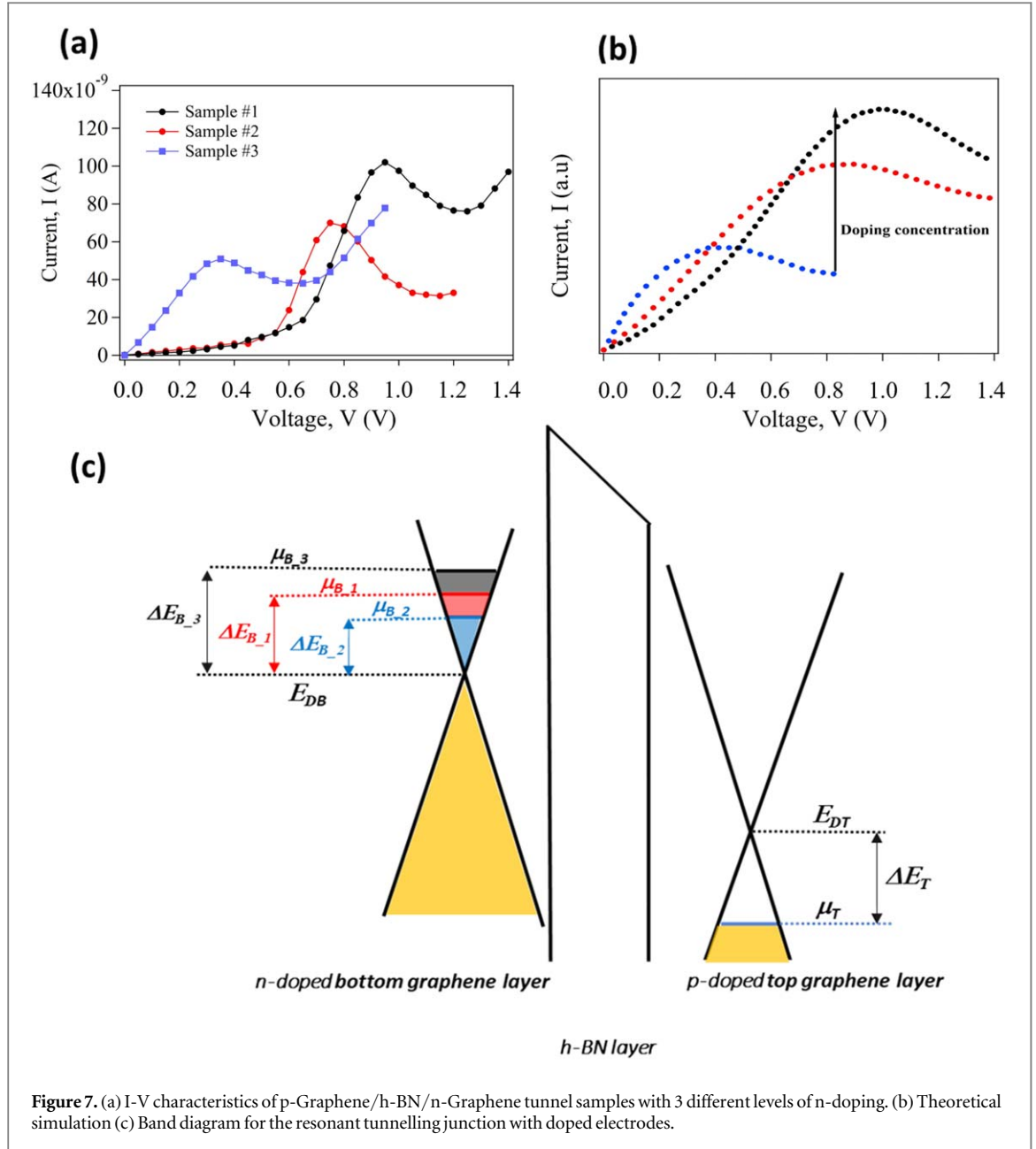


Figure 7. (a) I-V characteristics of p-Graphene/h-BN/n-Graphene tunnel samples with 3 different levels of n-doping. (b) Theoretical simulation (c) Band diagram for the resonant tunnelling junction with doped electrodes.

$$f_T(E) = [1 + e^{\left[\frac{E - \mu_T}{k_B T}\right]}]^{-1} \text{ and } f_B(E) = [1 + e^{\left[\frac{E - \mu_B}{k_B T}\right]}]^{-1} \quad (2)$$

The tunneling current can be simplified as,

$$I \propto \int_{\mu + eV}^{\mu} \text{DOS}_T(E) \text{DOS}_B(E - eV) T(E) [f(E) - f(E - eV)] dE \quad (3)$$

Where, $f(E)$ is the Fermi distribution function, $\text{DOS}_{T(B)}(E)$ is the density of states in the top (bottom) electrode, $T(E)$ is the transmission probability at the given energy. Figure 5(b) shows the tunneling current calculated for varying h-BN thicknesses according to equation (3). In the simulation, we assumed relativistic density of states of graphene, $\text{DOS}(E) \sim |E|$ and restricted the energy integral limits μ and $\mu + eV$, where μ is the chemical potential. It is also assumed that there is no in-plane momentum conservation, The calculated tunneling currents qualitatively agree very well with the experimental results for appropriate h-BN thicknesses.

4.2. Resonant tunneling with unequal doping

Here the same sequential processes were used for fabricating p-graphene/h-BN/n-graphene based device [84]. First n type graphene (n-graphene) was deposited using PECVD using NH_3 in addition to CH_4 on a Si/SiO₂ substrate. Next, through a mask with a circular opening, h-BN was deposited on previously deposited graphene

again using PECVD with ammonia borane as described before. Finally, the third p-type graphene (p-graphene) layer was deposited using another mask with a smaller opening.

The thermopower of p and n-graphene was measured using the analog-subtraction method developed in our laboratory. Two miniature thermocouples (Chromel (KP)/Au–7 at. % Fe (Au/Fe); 100 μm diameter) and a resistive heater were used for the measurements. The as deposited graphene was found to be p-type with the thermopower of $+60 \mu\text{V K}^{-1}$. In order to n-dope graphene, it was exposed to hydrazine. Figure 6(a) shows the thermopower response of graphene when exposed to hydrazine at room temperature. The downward arrows indicate where hydrazine was introduced to a pressure of 3, 7 and 10 Torr. After the first exposure to 3 Torr, the thermopower decreased and turned negative and eventually saturated at a value $\sim 10 \mu\text{V K}^{-1}$. Further exposure to the pressures of 7 Torr and 10 Torr resulted in saturating the thermopower at ~ -55 and $\sim -80 \mu\text{V K}^{-1}$ respectively. The n-doped graphene with ammonia shows the thermopower $\sim 250 \mu\text{V K}^{-1}$ (figure 6(b)).

Figure 7(a) shows the I-V characteristics of p-Graphene/h-BN/n-Graphene samples with 3 different levels of n-doping. The I-V curves of all three samples show the presence of a pronounced peak in the current corresponding to negative differential conductance (NDC) whose peak current value and the voltage value depend on the doping level of the n-layer. It is assumed that the doping level of the p-layer is the same as it's due to the intrinsic doping presumably due to an electrochemically mediated charge transfer process [85] under the ambient conditions. It can be seen that the peak current and the peak voltage increase when the doping level of the n-layer increases. Figure 7(b) shows the Bardeen tunneling model including the effect of doping in both graphene electrodes. As shown in the inset to figure 7(c), we assume that the top electrode is n-doped and the bottom electrode is p-doped, with chemical potentials $\mu_B = E_{DB} + \Delta E_B$ and $\mu_T = E_{DT} - \Delta E_T$ for specific ΔE_B and ΔE_T where E_{DB} and E_{DT} are the respective Dirac points [12, 86]. Both ΔE_B and ΔE_T depend not only on the doping of the graphene electrodes as described before, but also on the external bias voltage, V and the junction capacitance, C . [12, 87] The resonant condition arises when $eV = \Delta E_B + \Delta E_T$. The relativistic density of states of n- and p- doped graphene, $\text{DOS}(E) \sim |E \pm (E_D - E_F)|$ respectively, was assumed, where E_D is the Dirac point energy and E_F is the Fermi energy.

5. Conclusion

In conclusion, we have demonstrated a direct method for fabricating devices with atomically thin tunnel barriers by direct deposition of h-BN with graphene (doped and undoped) active electrode layers on a Si/SiO₂ substrate using a PECVD method. A variety of devices including unequally doped graphene electrodes separated by a thin h-BN layer were also fabricated by using different doping methods of these materials for the upper and lower electrodes. Our measurements of the electron tunnel current through the barrier demonstrate that the h-BN films act as a good tunnel barrier. Current-voltage measurements for different BN thicknesses and equally doped graphene based single barrier tunneling shows linear I-V characteristics at low bias but shows an exponential dependence at higher bias. The tunnelling devices consisting of unequally doped graphene with a single barrier shows resonant quantum tunneling with the presence of a pronounced peak in the current corresponding to negative differential conductance (NDC) whose peak current value and the voltage value depend on the doping levels. The results are explained according to the modified Bardeen tunneling model.

Acknowledgments

This work was partially supported by the U.S. Department of Energy, Office of Science, Basic Energy Sciences, under Award # DE-SC0019348. We also acknowledge the financial support provided by the Umm Al-Qura University.

Data availability statement

The data that support the findings of this study are available upon reasonable request from the authors.

ORCID iDs

Ali Alzahrani  <https://orcid.org/0000-0002-0032-6436>

Adel Alruqi  <https://orcid.org/0000-0003-0944-7717>

Bhupendra Karki  <https://orcid.org/0000-0002-9942-2056>

Milinda Kalutara Korallalage  <https://orcid.org/0000-0002-1356-7060>

Jacek Jasinski  <https://orcid.org/0000-0002-1297-6145>

References

- [1] Kim S M, Kim H J, Jung H J, Kim S H, Park J Y, Seok T J, Park T J and Lee S W 2019 Highly uniform resistive switching performances using two-dimensional electron gas at a thin-film heterostructure for conductive bridge random access Memory, *Acs Appl Mater Inter* **11** 30028–36
- [2] Zheng L and Fertig H A 1995 Wigner-crystal states for the 2-dimensional electron-gas in a double-quantum-well system *Phys. Rev. B* **52** 12282–90
- [3] Yang C L, Zhang J, Du R R, Simmons J A and Reno J L 2002 Zener tunneling between Landau orbits in a high-mobility two-dimensional electron gas *Phys. Rev. Lett.* **89** 076801
- [4] Geller M, Marquardt B, Lorke A, Reuter D, Wieck A D and Two-Dimensional A 2010 Electron gas as a sensitive detector for time-resolved tunneling measurements on self-assembled quantum dots *Nanoscale Res. Lett.* **5** 829–33
- [5] Popovic D, Fowler A B and Washburn S 1991 Resonant tunneling and hopping through a series of localized states in a 2-dimensional electron-gas *Phys. Rev. Lett.* **67** 2870–3
- [6] Feenstra R M, Jena Debdeep and Gu Gong 2012 Single-particle tunneling in doped graphene-insulator-graphene junctions *J. Appl. Phys.* **111** 043711
- [7] Hwan Lee S, Sup Choi M, Lee J, Ho Ra C, Liu X, Hwang E, Hee Choi J, Zhong J, Chen W and Jong Yoo W 2014 High performance vertical tunneling diodes using graphene/hexagonal boron nitride/graphene hetero-structure *Appl. Phys. Lett.* **104** 053103
- [8] Britnell L, Gorbachev R V, Geim A K, Ponomarenko L A, Mishchenko A, Greenaway M T, Fromhold T M, Novoselov K and Eaves, L S 2013 Resonant tunnelling and negative differential conductance in graphene transistors *Nat. Commun.* **4** 1794
- [9] Vanhoof C, Genoe J, Portal J C and Borghs G 1995 Charge accumulation in the 2-dimensional electron-gas emitter of a resonant-tunneling diode *Phys. Rev. B* **52** 1516–9
- [10] Lake Roger, Klimeck Gerhard and Datta Supriyo 1993 Rate equations from the Keldysh formalism applied to the phonon peak in resonant-tunneling diodes *Phys. Rev. B* **47** 6427
- [11] Roy T, Liu L, de la Barrera S, Chakrabarti B, Hesabi Z R, Joiner C A, Feenstra R M, Gu G and Vogel E M 2014 Tunneling characteristics in chemical vapor deposited graphene–hexagonal boron nitride–graphene junctions *Appl. Phys. Lett.* **104** 123506
- [12] Britnell L, Gorbachev R V, Geim A K, Ponomarenko L A, Mishchenko A, Greenaway M T, Fromhold T M, Novoselov K S and Eaves L 2013 Resonant tunnelling and negative differential conductance in graphene transistors *Nat. Commun.* **4** 1794
- [13] Lin Y C, Ghosh R K, Addou R, Lu N, Eichfeld S M, Zhu H, Li M Y, Peng X, Kim M J, Li L J, Wallace R M, Datta S and Robinson J A 2015 Atomically thin resonant tunnel diodes built from synthetic van der Waals heterostructures *Nat. Commun.* **6** 7311
- [14] Feng S, Liu C, Zhu Q, Su X, Qian W, Sun Y, Wang C, Li B, Chen M and Chen L 2021 An ultrasensitive molybdenum-based double-heterojunction phototransistor *Nat. Commun.* **12** 1–8
- [15] Cornescu A C 2019 High efficiency and high frequency resonant tunneling diode sources *Doctorial dissertation* University of Glasgow (<https://doi.org/10.5525/gla.thesis.76766>)
- [16] Wang S Y, Tan L Z, Wang W H, Louie S G and Lin N A 2014 Manipulation and characterization of aperiodical graphene structures created in a two-dimensional electron gas *Phys. Rev. Lett.* **113**
- [17] Castro Neto A H, Guinea F, Peres N M R, Novoselov K S and Geim A K 2009 The electronic properties of graphene *Rev. Mod. Phys.* **81** 109–62
- [18] Dasari B L, Nouri J M, Brabazon D and Naher S 2017 Graphene and derivatives - Synthesis techniques, properties and their energy applications *Energy* **140** 766–78
- [19] Akhtar M, Anderson G, Zhao R, Alruqi A, Mroczkowska J E, Sumanasekera G and Jasinski J B 2017 Recent advances in synthesis, properties, and applications of phosphorene *npj 2D Materials and Applications* **1** 5
- [20] Pop E, Varshney V and Roy A K 2012 Thermal properties of graphene: Fundamentals and applications *MRS Bull.* **37** 1273–81
- [21] Zhi C Y, Bando Y, Tang C C, Kuwahara H and Golberg D 2009 Large-scale fabrication of boron nitride nanosheets and their utilization in polymeric composites with improved thermal and mechanical properties *Adv. Mater.* **21** 2889
- [22] Worsley M A, Shin S J, Merrill M D, Lenhardt J, Nelson A J, Woo L Y, Gash A E, Baumann T F and Orme C A 2015 Ultra low density, monolithic WS₂, MoS₂, and MoS₂/graphene Aerogels *Acs Nano* **9** 4698–705
- [23] Cai Zhengyang, Liu Bilu, Zou Xiaolong and Cheng Hui-Ming 2018 Chemical vapor deposition growth and applications of two-dimensional materials and their heterostructures *Chem. Rev.* **118** 6091–133
- [24] Island J, Steele G A, van der Zant H S J and Castellanos-Gomez A 2015 Environmental Instability of Few-Layer Black Phosphorus *2D Mater.* **2** 011002
- [25] Alruqi A, Zhao R, Jasinski J and Sumanasekera G J N 2019 Graphene-WS₂ heterostructures by a lithography free method: their electrical properties *Nanotechnology* **30** 275704
- [26] Jayasingha R, Sherehiy A, Wu S-Y and Sumanasekera G U 2013 In Situ study of hydrogenation of graphene and new phases of localization between metal–insulator transitions *Nano Lett.* **13** 5098–105
- [27] Zhao R, Jayasingha R, Sherehiy A, Dharmasena R, Akhtar M, Jasinski J B, Wu S-Y, Henner V and Sumanasekera G U 2015 In Situ transport measurements and band gap formation of fluorinated graphene *The Journal of Physical Chemistry C* **119** 20150–5
- [28] Hibino H, Wang S, Orofeo C M and Suzuki S 2015 Synthesis and functionalization of two-dimensional materials: graphene, hexagonal boron nitride, and transition metal dichalcogenides *2015 22nd International Workshop on Active-Matrix Flatpanel Displays and Devices (AM-FPD)* 45–8
- [29] Eksik O, Gao J, Shojaee S A, Thomas A, Chow P, Bartolucci S F, Lucca D A and Koratkar N 2014 Epoxy nanocomposites with two-dimensional transition metal dichalcogenide additives *ACS Nano* **8** 5282–9
- [30] Wang X, Xing W, Feng X, Song L and Hu Y 2017 MoS₂/polymer nanocomposites: preparation, properties, and applications *Polym. Rev.* **57** 440–66
- [31] Novoselov K S, Mishchenko A, Carvalho A and Castro Neto A H 2016 2D materials and van der Waals heterostructures *Science* **353** aac9439
- [32] Iannaccone G, Bonaccorso F, Colombo L and Fiori G 2018 Quantum engineering of transistors based on 2D materials heterostructures *Nat. Nanotechnol.* **13** 183–91
- [33] Wang H, Liu F, Fu W, Fang Z, Zhou W and Liu Z 2014 Two-dimensional heterostructures: fabrication, characterization, and application *Nanoscale* **6** 12250–72
- [34] Alruqi A 2019 *2D materials based heterostructures: a lithography free method*, *Doctorial dissertation* University of Louisville
- [35] Britnell L et al 2012 Field-effect tunneling transistor based on vertical graphene heterostructures *Science* **335** 947
- [36] Gannett W, Regan W, Watanabe K, Taniguchi T, Crommie M F and Zettl A 2011 Boron nitride substrates for high mobility chemical vapor deposited graphene *Appl. Phys. Lett.* **98** 242105

- [37] Geim A K and Grigorieva I V 2013 Van der Waals heterostructures *Nature* **499** 419
- [38] Georgiou T, Jalil R, Belle B D, Britnell L, Gorbachev R V, Morozov S V, Kim Y-J, Gholinia A, Haigh S J, Makarovskiy O, Eaves L, Ponomarenko L A, Geim A K, Novoselov K S and Mishchenko A 2012 Vertical field-effect transistor based on graphene–WS₂ heterostructures for flexible and transparent electronics *Nat. Nanotechnol.* **8** 100
- [39] Yu W J, Liu Y, Zhou H, Yin A, Li Z, Huang Y and Duan X 2013 Highly efficient gate-tunable photocurrent generation in vertical heterostructures of layered materials *Nat. Nanotechnol.* **8** 952
- [40] Yu W J, Li Z, Zhou H, Chen Y, Wang Y, Huang Y and Duan X 2012 Vertically stacked multi-heterostructures of layered materials for logic transistors and complementary inverters *Nat. Mater.* **12** 246
- [41] Myoung N, Seo K, Lee S J and Ihm G 2013 Large current modulation and spin-dependent tunneling of vertical graphene/MoS₂ heterostructures *ACS Nano* **7** 7021–7
- [42] Lan C, Li C, Wang S, He T, Zhou Z, Wei D, Guo H, Yang H and Liu Y 2017 Highly responsive and broadband photodetectors based on WS₂–graphene van der Waals epitaxial heterostructures *J. Mater. Chem. C* **5** 1494–500
- [43] He J, Kumar N, Bellus M Z, Chiu H-Y, He D, Wang Y and Zhao H 2014 Electron transfer and coupling in graphene–tungsten disulfide van der Waals heterostructures *Nat. Commun.* **5** 5622
- [44] Koppens F H L, Mueller T, Avouris P, Ferrari A C, Vitiello M S and Polini M 2014 Photodetectors based on graphene, other two-dimensional materials and hybrid systems *Nat. Nanotechnol.* **9** 780
- [45] Lin Y-F, Li W, Li S-L, Xu Y, Aparecido-Ferreira A, Komatsu K, Sun H, Nakaharai S and Tsukagoshi K 2014 Barrier inhomogeneities at vertically stacked graphene-based heterostructures *Nanoscale* **6** 795–9
- [46] Watt F, Bettiol A, Van Kan J, Teo E J and Breese M B H 2005 Ion beam lithography and nanofabrication: a review *Int. J. Nanosci.* **4** 269–86
- [47] Wang H and Wu T 2012 A general lithography-free method of microscale/nanoscale fabrication and patterning on Si and Ge surfaces *Nanoscale Res. Lett.* **7** 110
- [48] Bao W et al 2010 Lithography-free fabrication of high quality substrate-supported and freestanding graphene devices *Nano Res.* **3** 98–102
- [49] Cho Shinuk, Leea Kwanghee, Yuen Jonathan, Wang Guangming, Moses Daniel, Heeger Alan J., Surin Mathieu and Lazzaroni Roberto 2006 Thermal annealing-induced enhancement of the field-effect mobility of regioregular poly(3-hexylthiophene) films *J. Appl. Phys.* **100** 114503
- [50] Seo J H, Park J H, Kim S I, Park B J, Ma Z, Choi J and Ju B K 2014 Nanopatterning by laser interference lithography: applications to optical devices *J. Nanosci. Nanotechnol.* **14** 1521–32
- [51] Khadpekar A J et al 2019 Low cost and lithography-free stamp fabrication for microcontact printing *Sci. Rep.* **9** 1024
- [52] Wood J D, Schmucker S W, Lyons A S, Pop E and Lyding J W 2011 Effects of polycrystalline Cu substrate on graphene growth by chemical vapor deposition *Nano Lett.* **11** 4547–54
- [53] Zhang Y, Gomez L, Ishikawa F N, Madaria A, Ryu K, Wang C A, Badmaev A and Zhou C W 2010 Comparison of graphene growth on single-crystalline and polycrystalline ni by chemical vapor deposition *J. Phys. Chem. Lett.* **1** 3101–7
- [54] Yao Y G and Wong C P 2012 Monolayer graphene growth using additional etching process in atmospheric pressure chemical vapor deposition *Carbon* **50** 5203–9
- [55] Zhang Y F, Gao T, Xie S B, Dai B Y, Fu L, Gao Y B, Chen Y B, Liu M X and Liu Z F 2012 Different growth behaviors of ambient pressure chemical vapor deposition graphene on Ni(111) and Ni films: A scanning tunneling microscopy study *Nano Res.* **5** 402–11
- [56] Song W, Jeon C, Kim S Y, Kim Y, Kim S H, Lee S I, Jung D S, Jung M W, An K S and Park C Y 2014 Two selective growth modes for graphene on a Cu substrate using thermal chemical vapor deposition *Carbon* **68** 87–94
- [57] Faggio G, Capasso A, Messina G, Santangeo S, Dikonimos T, Gagliardi S, Giorgi R, Morandi V, Ortolani L and Lisi N 2013 High-temperature growth of graphene films on copper foils by ethanol chemical vapor deposition *J. Phys. Chem. C* **117** 21569–76
- [58] Gao T, Xie S B, Gao Y B, Liu M X, Chen Y B, Zhang Y F and Liu Z F 2011 Growth and atomic-scale characterizations of graphene on multifaceted textured Pt foils prepared by chemical vapor deposition *ACS Nano* **5** 9194–201
- [59] Yao Y G, Li Z, Lin Z Y, Moon K S, Agar J and Wong C P 2011 Controlled growth of multilayer, few-layer, and single-layer graphene on metal substrates *J. Phys. Chem. C* **115** 5232–8
- [60] Guermoune A, Chari T, Popescu F, Sabri S S, Guillemette J, Skulason H S, Szkopek T and Sijaj M 2011 Chemical vapor deposition synthesis of graphene on copper with methanol, ethanol, and propanol precursors *Carbon* **49** 4204–10
- [61] Dong X C, Wang P, Fang W J, Su C Y, Chen Y H, Li L J, Huang W and Chen P 2011 Growth of large-sized graphene thin-films by liquid precursor-based chemical vapor deposition under atmospheric pressure *Carbon* **49** 3672–8
- [62] Yu Q K, Lian J, Siriponglert S, Li H, Chen Y P and Pei S S 2008 Graphene segregated on Ni surfaces and transferred to insulators *Appl. Phys. Lett.* **93** 113103
- [63] Reina A, Jia X T, Ho J, Nezich D, Son H B, Bulovic V, Dresselhaus M S and Kong J 2009 Layer area, few-layer graphene films on arbitrary substrates by chemical vapor deposition *Nano Lett.* **9** 3087–3087
- [64] Kim K S, Zhao Y, Jang H, Lee S Y, Kim J M, Kim K S, Ahn J H, Kim P, Choi J Y and Hong B H 2009 Large-scale pattern growth of graphene films for stretchable transparent electrodes *Nature* **457** 706–10
- [65] Li X S, Zhu Y W, Cai W W, Borysiak M, Han B Y, Chen D, Piner R D, Colombo L and Ruoff R S 2009 Transfer of large-area graphene films for high-performance transparent conductive electrodes *Nano Lett.* **9** 4359–63
- [66] Cai C Y, Jia F X, Li A L, Huang F, Xu Z H, Qiu L Z, Chen Y Q, Fei G T and Wang M 2016 Crackless transfer of large-area graphene films for superior-performance transparent electrodes *Carbon* **98** 457–62
- [67] Malesev A, Vitchev R, Schouteden K, Volodin A, Zhang L, Tendeloo G V, Vanhulsel A and Haesendonck C V 2008 Synthesis of few-layer graphene via microwave plasma-enhanced chemical vapour deposition *Nanotechnology* **19** 305604
- [68] Bo Z, Yang Y, Chen J, Yu K, Yan J and Chen K 2013 Plasma-enhanced chemical vapor deposition synthesis of vertically oriented graphene nanosheets *Nanoscale* **5** 5180–204
- [69] Yamada T, Kim J, Ishihara M and Hasegawa M 2013 Low-temperature graphene synthesis using microwave plasma CVD *J. Phys. D* **46** 063001
- [70] Chen S, Gao M, Cao R, Du H, Yang J, Zhao L and Ma Z 2014 Hydrogen-free synthesis of graphene–graphitic films directly on Si substrate by plasma enhanced chemical vapor deposition *J. Mater. Sci., Mater. Electron.* **26** 1485–93
- [71] Woehrl N, Ochedowski O, Gottlieb S, Shibasaki K and Schulz S 2014 Plasma-enhanced chemical vapor deposition of graphene on copper substrates *AIP Adv.* **4** 047128
- [72] Othman M, Ritikos R, Hafiz S M, Khanis N H, Rashid N M A and Rahman S A 2015 Low-temperature plasma-enhanced chemical vapour deposition of transfer-free graphene thin films *Mater. Lett.* **158** 436–8

- [73] Xu Z G, Zheng R J, Khanaki A, Zuo Z and Liu J L 2015 Direct growth of graphene on in situ epitaxial hexagonal boron nitride flakes by plasma-assisted molecular beam epitaxy *Appl. Phys. Lett.* **107**
- [74] Sun J, Chen Y, Cai X, Ma B, Chen Z, Priyadarshi M K, Chen K, Gao T, Song X, Ji Q, Guo X, Zou D, Zhang Y and Liu Z 2015 Direct low-temperature synthesis of graphene on various glasses by plasma-enhanced chemical vapor deposition for versatile, cost-effective electrodes *Nano Res.* **8** 3496–504
- [75] Britnell Liam *et al* 2012 Atomically thin boron nitride: a tunnelling barrier for graphene devices *Nano Lett.* **12** 1707–10
- [76] Qian F, Deng J, Xiong F, Dong Y, Hu L, Pan G, Wang Q, Xie Y, Sun J and Xu C 2020 Direct Growth of High Quality Graphene Nanowalls on Dielectric Surfaces By Plasma-Enhanced Chemical Vapor Deposition For Photo Detection *Opt. Mater. Express* **10** 2909–18
- [77] Han T, Liu H, Chen S, Chen Y, Wang S and Li Z 2020 Fabrication and Characterization of MoS₂/h-BN and WS₂/h-BN Heterostructures *Micromachines* **11** 1114
- [78] Rong Z, Meysam A, Adel A, Ruchira D, Jacek B J, Rukshan M T and Gamini U S 2017 Electrical transport properties of graphene nanowalls grown at low temperature using plasma enhanced chemical vapor deposition *Mater. Res. Express* **4** 055007
- [79] Rong Zhao Meysam, Ahktar Adel, Alruqi Ruchira, Dharmasena Jacek B, Jasinski Rukshan M, Thantirige and Gamini U Sumanasekera 2017 Electrical transport properties of graphene nanowalls grown at low temperature using plasma enhanced chemical vapor deposition *Mater. Res. Express* **4** 055007
- [80] Koepke Justin C. *et al* 2016 Role of pressure in the growth of hexagonal boron nitride thin films from ammonia-borane *Chem. Mater.* **28** 4169–79
- [81] Babenko V, Lane G, Koos A A, Murdock A T, So K, Britton J, Meysami S S, Moffat J and Grobert N 2017 Time Dependent Decomposition Of Ammonia Borane For The Controlled Production Of 2d Hexagonal Boron Nitride *Sci. Rep.* **7** 1–12
- [82] Ferrari A C, Meyer J C, Scardaci V, Casiraghi C, Lazzeri M, Mauri F, Piscanec S, Jiang D, Novoselov K S, Roth S and Geim A K 2006 Raman spectrum of graphene and graphene layers *Phys. Rev. Lett.* **97**
- [83] Alruqi Adel, Rajib Khan Musa Md, Zhao Rong, Zhang Congyan, Jasinski Jacek B., Yu Ming and Sumanasekera Gamini 2019 Layer-dependent hydrazine adsorption properties in few-layer Ws₂ *J. Phys. Chem. C* 2019 **123** 20 13167–73
- [84] Babu Marahatta Anant 2019 Technologies, effect of n-type dopant nitrogen in the structure and atomic charges distribution of monolayer graphene sheet: a dft analysis *IJPSAT* **16** 01–13
- [85] Chakrapani V, Angus J C, Anderson A B, Wolter S D, Stoner B R and Sumanasekera G U 2007 Charge transfer equilibria between diamond and an aqueous oxygen electrochemical redox couple *Science* **318** 1424–30
- [86] Mishchenko A *et al* 2014 Twist-controlled resonant tunnelling in graphene/boron nitride/graphene heterostructures *Nat. Nanotechnol.* **9** 808–13
- [87] Kang H, Yun Y, Park J, Kim J, Truong T K, Kim J G, Park N, Yun H, Lee S W, Lee Y H and Suh D 2015 Quantum hall conductance of graphene combined with charge-trap memory operation *Nanotechnology* **26** 345202